Sensitivity thermal analysis in the laser-assisted tape placement process

Marta Perez, Anaïs Barasinski, Benoît Courtemanche, Chady Ghnatios, Francisco Chinesta

Sensitivity thermal analysis in the laser-assisted tape placement process

Marta Perez[1], Anais Barasinski[1,*], Benoit Courtemanche[2], Chady Ghnatios[3] and Francisco Chinesta[4]

[1] GEM, UMR CNRS-Centrale Nantes, 1 rue de la Noe, BP 92101, F-44321 Nantes cedex 3, France
[2] CETIM – Technocampus Composites, ZI du Chaffault, Chemin du Chaffault, 44340 Bouguenais, France
[3] Notre Dame University Louaize, P.O. Box 72, Zouk Mikael, Zouk Mosbeh, Lebanon
[4] ESI Group Chair @ PIMM, ENSAM ParisTech, 151 Boulevard de l'Hôpital, 75013 Paris, France

Correspondence: Email: anais.barasinski@ec-nantes.fr.

Abstract: Nowadays, the production of large pieces made of thermoplastic composites is an industrial challenging issue as there are yet several difficulties associated to their processing. The laser-assisted tape placement (LATP) process is an automated manufacturing technique to produce long-fiber reinforced thermoplastic matrix composites. In this process, a tape is placed and progressively welded on the substrate. The main aim of the present work is to solve an almost state of the art thermal model by using an efficient numerical technique, the so-called Proper Generalized Decomposition (PGD) that considers parameters (geometrical and material) as model extra-coordinates. Within the PGD rationale the parametric temperature field is expressed in a separated form, as a finite sum of functional products, where each term depends on a single coordinate (space, time or each one of the parameters considered as extra-coordinates). Such a separated representation allows the explicit expression of the sensitivity fields, from the temperature derivative with respect to each parameter. These sensitivity fields represent a very valuable methodology to analyze and establish the influence of the critical input parameters on the thermal response, and therefore, for performing process optimization and control, as well as for evaluating the effect of parameters variability on the thermal response.

Keywords: composites; automated tape placement; thermal modeling; Proper Generalized Decomposition; statistics analysis; uncertainty propagation

1. Introduction

The context of this study is the LATP process, that consists in an automated filament winding process designed to produce composite parts with a thermoplastic matrix. A fiber-reinforced composite is continuously laid-down onto the previously laid tapes around a mandrel, while the tape is heated up by the laser in order to bond it to the substrate.

The main difficulty when using this technology lies in the heating control of the tape and the variability of the material, which affects the quality and properties of the part. The heating and cooling cycles generate very high temperature gradients (between 300 and 1400 °C/s), applied to a thin prepreg material (about 150 μm). These particular conditions hinder the use, in LATP, of autoclave conventional control and measurements methods. In addition, the tape may also exhibit irregularities in terms of fiber volume fraction, porosity, roughness, and thickness which may vary along the length of the prepreg tape. In this case, the tape may not heat uniformly, therefore won't weld as expected with the consequent impact on the part properties and performances.

Many recents works addressed modeling and simulation issues, as well as experimental characterization and validation [1–6]. The main difficulties from the modeling point of view come from the multiple scales and physics encountered in LATP processes. First, in the laser/composite interaction the penetration depth is extremely small, two or three fiber rows, creating a high thermal localization difficult to model and to resolve numerically.

The heat partition between the incoming tape and the substrate represents another issue, because there are multiple reflections between them, and absorption depends strongly on the microstructure (fibers distribution, exhibiting large variability at that scale), on the fiber orientation and also on the electromagnetic material properties. Simulation is usually performed by using ray-tracing (geometric optics) [7, 8], even if the relation between the wavelength and the fiber diameter compromises the validity is many cases. Other alternative approches using more general electromagnetic models were addressed in [9, 10].

Then, consolidation is facilitated by the compression provided by a roller. The thermo-mechanical coupling is of major relevance, because the squeeze flow at the tape/substrate interface depends on the roller stiffness, its thermal properties and the applied pressure. The roller/composite interaction is difficult to simulate, due to the small tape and substrate thicknesses require levels of resolution difficult to attain by using standard mesh-based discretization techniques. Here, in-plane-out-of-plane decompositions involved in the PGD-based solvers were successfully employed in our former works [11, 12].

The thermal model, and more concretely the thermo-rheological coupling, is the key factor when modeling and simulating consolidation at the tape/substrate interface. First, the description of interface roughness remains an open issue [13–15]. Then the squeeze flow at the interface scale, where asperities are composed of resin (whose viscosity is largely affected by the temperature) that can flow under the applied compression [16–18], and fibers, that require local accommodation and the flow of the resin located in between, remains an open issue from the modeling and simulation viewpoints. Moreover, the connexion between interface morphology and thermal resistance is of major relevance to ensure accurate time-dependent thermal evaluations, required for evaluating the time-evolution of viscosity and also the molecular diffusion that allows recovering similar properties at the interface level that the ones existing in the bulk.

Finally, modeling and simulating the cooling process allows predicting the residual stresses installation, that are responsible of the final part distortions [11, 12, 19]. The main issue again in the very degenerated geometries, where the thickness is orders of magnitude smaller that the other characteristic dimensions, making difficult the use of accurate 3D finite element simulations.

As just described LATP involves many scales, and many physics. The issue related to the multiple scales can be efficiently addressed using adapted numerical techniques able to resolve all the involved scales. The issue related to the multi-physics nature can also be accurately accounted, however, the existence of many models with their own parameters makes difficult to extract the most critical, explicative or significant parameters, and more precisely, where and when each one expresses its influence.

One could think that addressing this issue only requires performing a rich enough DoE (design of experiments), and from it making a parametric study for extracting all the desired information. However, when the number of parameters increases the accuracy provided by a DoE is not enough for performing precise predictions.

The main aim of the present work is to solve an almost state of the art thermal model by using an efficient numerical technique that considers parameters (geometrical and material) as model extra-coordinates, the so-called Proper Generalized Decomposition (PGD). Within the PGD rationale the parametric temperature field is expressed in a separated form, as a finite sum of functional products, where each term depends on a single coordinate (space, time or each one of the parameters considered as extra-coordinates). Such a separated representation allows the explicit expression of the sensitivity fields, from the temperature derivative with respect to each parameter. These sensitivity fields represent a very valuable methodology to analyze and establish the influence of the critical input parameters on the thermal response, and therefore, for performing process optimization and control.

Moreover, having such a parametric solution allows quantifying the effects of materials and/or process parameters variability, because as highlighted latter, real properties are statistically distributed. Again, the availability of a parametric solution allows propagating uncertainty or variability in almost real-time.

The present work does not propose neither models nor simulation tools, it considers state of the art models, applies an advanced simulation tool, the Proper Generalized Decomposition (PGD) for calculating a parametric temperature, and then it proposes a new methodology for providing an exhaustive analysis on the critical parameters influencing the process (sensitivity analysis) as well as a very efficient uncertainty propagator, able to address material and process variability, and evaluating their impact on the process. In this work, we study the influence of material parameters variability into the thermal behaviour during the LATP process from the data reported in [20].

The experimental validation of the main conclusions of the present works constitutes a work in progress. As just commented, here we are considering almost state of the art models, and consequently we are confident on the pertinence of the main tendencies derived from our numerical analysis, as soon as models are expected being pertinent at least at the first order.

The present article is structured in three main parts. The first concerns the experimental characterization of the tapes as well as of its variability. Then, the second introduces parameters in the representative thermal model and computes the parametric temperature field. Finally, the third part analyses the influence of the input material parameters on the thermal response and perform a statistical analysis related to the material and process variability.

2. Characterization of the material and its variability

In this study, two different materials were chosen: material A (55% AS4/PEEK) and material B (50% HTS45/PEEK). Rings were manufactured consecutively by using the CETIM deposition machine, located in the Technocampus EMC2 at Nantes (France). Each ring needed approximately 4.4 m of tape, which correspond about 6 tape layers (Figure 1). Two main data were collected: temperature evolution, measured with a thermal camera (FLIR T660) and microscopic analysis of the cross-section of tapes before processing them. The process parameters were set to: circumferential velocity of 7 m/min, laser power of 1000 W and the pressure applied to the compression roller was set to 2 bars.

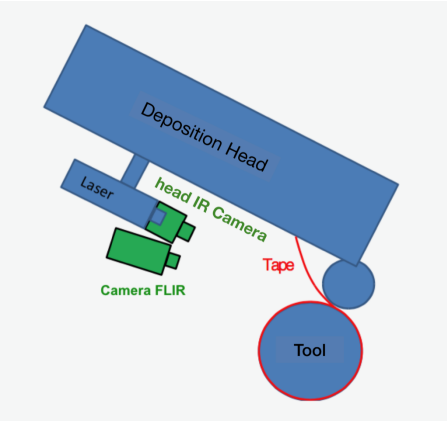

Figure 1. Ring fabrication scheme.

The image analysis is used to observe the microstructure of the material to eventually define the actual properties based on the observation of different phases. The analysis of these properties is then used to simulate the composite manufacturing processes. This section addresses the characterization, as accurate as possible, of the material parameters from the microcut images.The aim is obtaining information such as, fiber volume fraction (FVF), thickness and homogenized thermal conductivity tensor.

An active contour model (also called snake in computer vision) was used in order to find the contour of the pre-impregnated (prepreg) composite tape. A snake consists of a deformable spline minimizing energy and on which image forces apply pushing it towards the object contour, in the present case the tape contour. This method looks for minimizing the energy and requires the knowledge of the desired contour shape beforehand. This allowed to obtain a mask to detect the prepreg in the image. To detect the fibers in the image, the color image is converted to a gray-scale image. The gray scale image is then converted to a binary image based on a set threshold object detection method. The thresholding method replaces each pixel in an image with a black pixel if the image intensity is lower than a given value.

In [21], the size of a RVE (representative volume element) for a typical carbon fiber polymer was established and it was concluded that the minimum size is $\delta = \frac{L}{R} = 50$, being L the side of the element and R the fiber radius. This leads in our case, with a fiber diameter of around 7 μm, a RVE whose size is equal to the thickness of the prepreg. This issue is discussed later when calculating effective (homogenized) thermal properties.

2.1. *Fiber volume fraction*

The fiber volume fraction (FVF) is the percentage of fiber volume in the entire volume of the fiber-reinforced composite material. For each microscopic cross-section, FVF was measured for 25 RVE in each cross-section of material A and material B. For one RVE, the pixels whose value was equal to 1, that indicates a part of a fiber, were summed up and divided by all the pixels contained in the RVE leading to the fiber volume fraction. Figure 2 plots the distribution of FVF for material A and material B and gives an average value of 46% in the case of material B and 49% for material A.

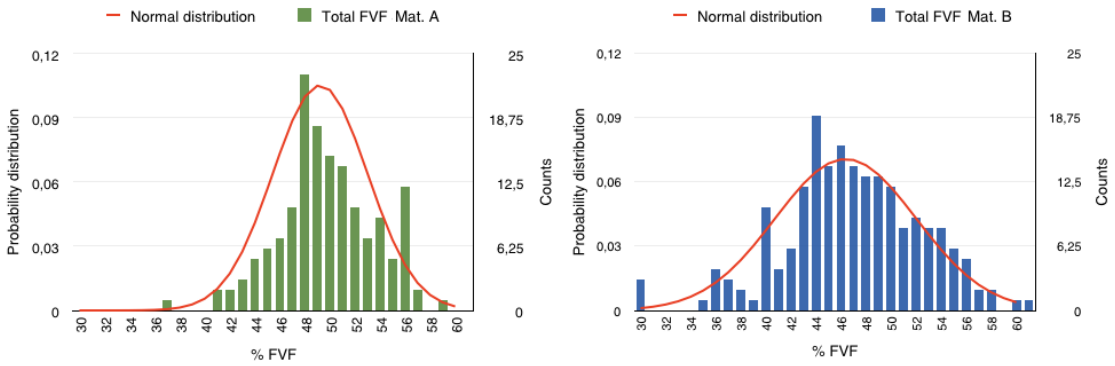

Figure 2. Fiber volume fraction distribution for material A (green) and material B (blue).

2.2. *Thickness*

The thickness was measured through the z-axis (vertical direction in Figure 1) and along the prepreg's width (represented by coordinate y). The results show an important variation in the thickness in the case of prepreg B, while for material A the thickness is more homogeneous. Figure 3 confirms this observation as the distribution of the thickness for all the material A samples are around 140 μm while for material B, the data is more dispersed.

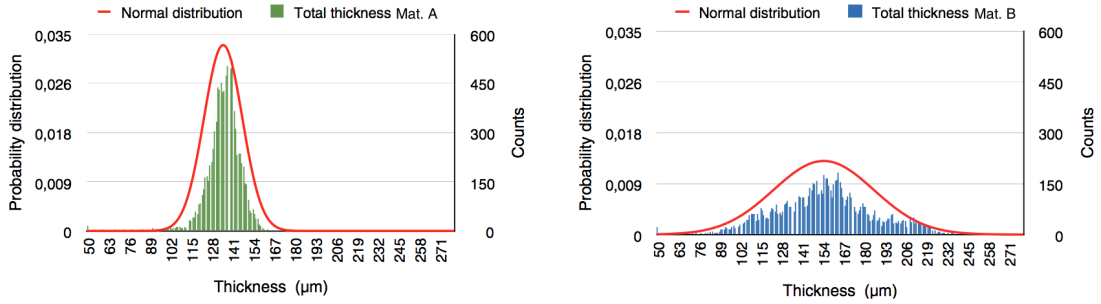

Figure 3. Thickness distribution for material A (green) and material B (blue).

2.3. *Homogenized thermal conductivity*

Due to the noticed microscopic heterogeneity, the macroscopic thermal modeling requires a homogenized thermal conductivity that depends on the microscopic details. As considered in our

former work [22], we can define the macroscopic temperature gradient ∇T at the elementary volume

$$\nabla T \;=\; \langle \mathbf{g}(\mathbf{x}) \rangle \;=\; \frac{1}{|\omega|} \int_{\omega} \mathbf{g}(\mathbf{x})\, d\mathbf{x}, \tag{1}$$

where $\mathbf{g}(\mathbf{x})$ denotes the microscopic temperature gradient. Following usual computational homogenization, we assume the existence of a localization tensor $\mathbf{L}(\mathbf{x})$ relating the macroscopic temperature gradient ∇T with the microscopic local temperature gradient $\mathbf{g}(\mathbf{x})$, such that

$$\mathbf{g}(\mathbf{x}) = \mathbf{L}(\mathbf{x}) \cdot \nabla T. \tag{2}$$

As previously indicated, due to the small tape thickness the elementary volume considered for calculating the effective thermal conductivity involves the entire tape thickness, with a width and length large enough for ensuring that the effective thermal properties remain almost stable with respect to the variation of these dimensions.

Now, we consider the microscopic heat flux $\mathbf{q}(\mathbf{x})$ according to the Fourier's law

$$\mathbf{q}(\mathbf{x}) \;=\; -\mathbf{k}(\mathbf{x}) \cdot \mathbf{g}(\mathbf{x}), \tag{3}$$

and its macroscopic counterpart $\mathbf{Q}$ that reads

$$\mathbf{Q} \;=\; \langle \mathbf{q}(\mathbf{x}) \rangle \;=\; -\langle \mathbf{k}(\mathbf{x}) \cdot \mathbf{g}(\mathbf{x}) \rangle \;=\; -\langle \mathbf{k}(\mathbf{x}) \cdot \mathbf{L}(\mathbf{x}) \rangle \cdot \nabla T, \tag{4}$$

from which the homogenized thermal conductivity can be defined from

$$\mathbf{K} = \; \langle \mathbf{k}(\mathbf{x}) \cdot \mathbf{L}(\mathbf{x}) \rangle. \tag{5}$$

As $\mathbf{k}(\mathbf{x})$ is perfectly known everywhere in the RVE ω, the definition of the homogenized thermal conductivity tensor only requires the computation of the localization tensor $\mathbf{L}(\mathbf{x})$. We consider the general 2D case that involves the solution of two boundary value problems related to the steady state heat transfer model in the microscopic domain ω for two different boundary conditions on $\partial\omega$:

$$\begin{cases} \nabla \cdot \left(\mathbf{k}(\mathbf{x}) \cdot \nabla \Theta^1(\mathbf{x}) \right) \;=\; 0 \\ \Theta^1(\mathbf{x} \in \partial\omega) = y \end{cases} \tag{6}$$

and

$$\begin{cases} \nabla \cdot \left(\mathbf{k}(\mathbf{x}) \cdot \nabla \Theta^2(\mathbf{x}) \right) \;=\; 0 \\ \Theta^2(\mathbf{x} \in \partial\omega) = z \end{cases}. \tag{7}$$

Thus, the localization tensor results finally:

$$\mathbf{L}(\mathbf{x}) \;=\; \left(\nabla \Theta^1(\mathbf{x}) \quad \nabla \Theta^2(\mathbf{x}) \right). \tag{8}$$

To obtain the macroscopic homogenized thermal conductivity tensor we analyzed 150 microstructures in the case of material A and 196 for the material B. The carbon fiber transverse conductivity was set to $k_f = 0.8$ W/mK [23–26] and the matrix conductivity $k_m = 0.2$ W/mK. The homogenized thermal conductivity distribution along the width and the thickness are depicted in Figures 4 and 5 respectively.

2.4. Variability of the material

The main information extracted from the aforementioned image analysis is listed in Tables 1 and 2. This data is the input parameters for the thermal model and the stochastic analysis developed in Sections 3 and 4.

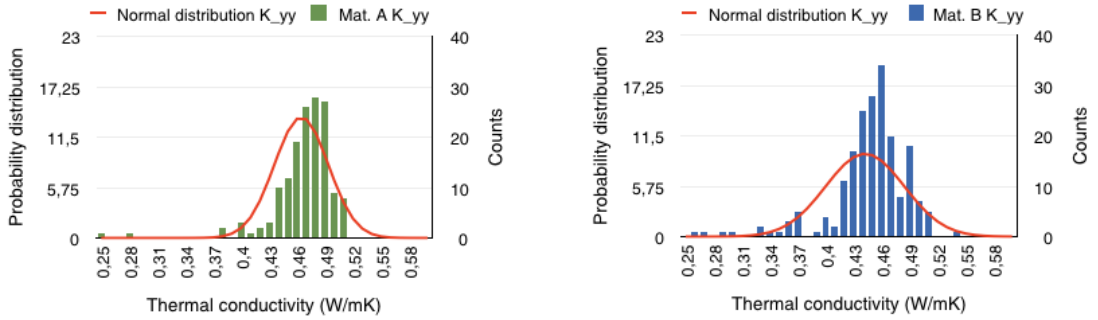

Figure 4. Through-width thermal conductivity distribution for material A (green) and material B (blue).

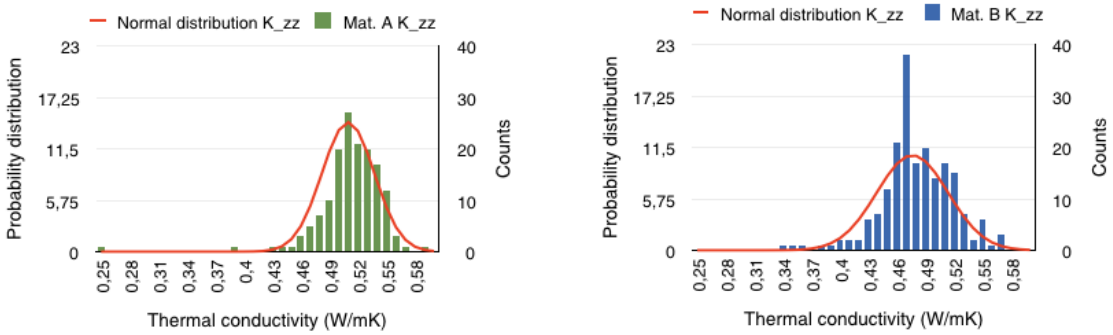

Figure 5. Through-thickness thermal conductivity distribution for material A (green) and material B (blue).

Table 1. Parameters variability for material A.

Parameter	Mean, μ	Std dev, σ	μ/σ (%)
FVF (%)	49.2	3.79	7.7
Thickness (μm)	135.2	12.06	8.9
K_{yy} (W/mK)	0.465	0.029	6.2
K_{zz} (W/mK)	0.510	0.028	5.4

Table 2. Parameters variability for material B.

Parameter	Mean, μ	Std dev, σ	μ/σ (%)
FVF (%)	46.4	5.64	12.2
Thickness (μm)	154.6	31.58	20.4
K_{yy} (W/mK)	0.442	0.042	9.5
K_{zz} (W/mK)	0.476	0.038	7.9

3. Deterministic thermal model

The objective of this section is to obtain the steady state temperature in a coordinate system attached to the placement head, which is assumed to move with a constant velocity. For a given number of plies, this temperature field can be used to reconstruct the thermal history in any material point. In these conditions each material point experiences the same thermal history during the process. It is progressively heated when approaching the laser, it reaches its maximum temperature when the laser applies directly on it and it cools down relatively fast when getting far from the heat source, reaching the ambient temperature before the next pass, when placing the next layer. Therefore, the laser and the roller are kept fixed and the material is assumed moving with a speed $\mathbf{v}$ in the opposite direction to the one of the laser and compression head. On the other hand, before experiencing the bonding the interface between the incoming layer and the substrate is modeled as a perfect insulation, to express the lack of contact between the incoming tape and the substrate.

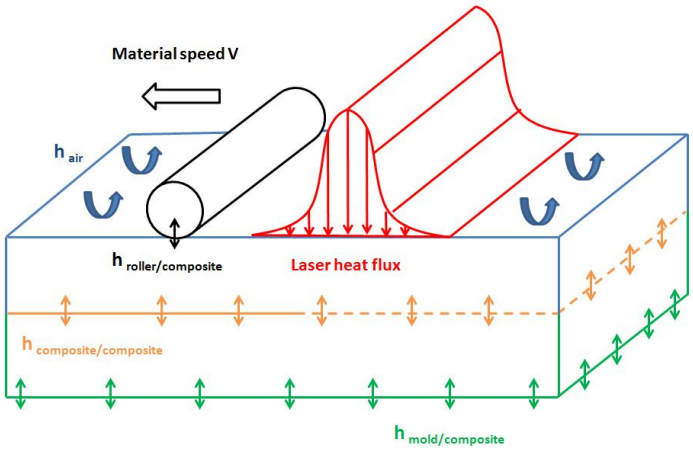

Figure 6. Simulation geometry and boundary conditions.

In the material domain, consisting in the substrate (plies already placed) and the incoming layer, defining the domain $\Omega = [0, L_x] \times [0, L_y] \times [0, L_z]$ as depicted in Figure 6, we solve the following heat problem widely considered when modelling ATP processes:

$$\rho C_p(\mathbf{v} \cdot \nabla T) = \nabla \cdot (\mathbf{K} \cdot \nabla T) \tag{9}$$

where T is the temperature, ρ is the density, C_p is the heat capacity, $\mathbf{K}$ is the homogenized anisotropic conductivity tensor and $\mathbf{v}$ is the velocity of the laminate with respect to the laser. The heating source is modeled as a surface flux. The convective boundary conditions with the air, roller and the mold, are expressed from

$$\mathbf{q}(\mathbf{x}, t) \cdot \mathbf{n} = h(T_{amb} - T(\mathbf{x}, t)) \tag{10}$$

where $\mathbf{q}$ is the heat flux, h is the heat transfer coefficient, T_{amb} is the ambient temperature, $T(\mathbf{x}, t)$ is the temperature on the boundary when the convective exchange operates between composite and roller, composite and air or composite and working plane. Convective exchanges scale with coefficient h that at its turn depends on the existing conditions in the systems exchanging heat. It is also assumed that at the boundary representing the incoming material the temperature corresponds to the ambient one,

whereas in the opposite boundary, where the material leaves the domain, the temperature is almost stabilized and consequently the heat flux vanishes.

It is important to note that numerical techniques employed in this paper perfectly work when addressing nonlinear models. An accurate solution of the ATP thermal model requires considering the temperature dependence of thermal parameters, however, as indicated in the introduction, here we are not interested in evaluating accurately the temperature field, but only the sensitivity of that field to the thermal parameters as well as analyzing the impact of variability. Thus, fine tuning and nonlinear modeling remain of second order as it was proved in our preliminary numerical tests carried out before considering the linear model.

3.1. Proper Generalized Decomposition

In order to solve a single multidimensional problem instead of running one simulation for each choice of the analyzed material parameters, we are going to introduce the material parameters as extra-coordinates in the thermal model. The difficulties related to the increase in the model's multidimensionality can be circumvented by using a separated representation [27, 28]. The Proper Generalized Decomposition (PGD) [29, 30] is an "a priori" model order reduction technique based on the use of separated representations in order to ensure that the complexity scales linearly with the model dimensionality. It consists of expressing the unknown field as a finite sum of functional products, i.e., expressing a generic multidimensional function $u(x_1, \cdots, x_d)$ as,

$$u(x_1, \cdots, x_d) \approx \sum_{i=1}^{i=N} X_i^1(x_1) \cdots X_i^d(x_d). \tag{11}$$

In the case of the thermal model presented above it involves as coordinates the space $\mathbf{x}$, the homogenized components of the conductivity tensor $\mathbf{K}$ (assumed a diagonal tensor since we are using only unidirectional prepregs), the tape thickness e and the specific heat ρC_p (the last is included as extra-coordinate because the noticed fibers weight fraction variability depending on the material supplier). By denoting by $\mathbf{x}$ the in plane coordinates (x,y), the temperature separated representation reads

$$T(\mathbf{x}, z, k_{yy}, k_{zz}, e, \rho C_p) \approx$$

$$\sum_{i=1}^{i=N} X_i(\mathbf{x}) \cdot Z_i(z) \cdot K_i^{yy}(k_{yy}) \cdot K_i^{zz}(k_{zz}) \cdot E_i(e) \cdot R_i(\rho C_p) \tag{12}$$

that results in a problem defined in a high-dimensional space, which in the more general 3D case involves 7 dimensions but whose computational complexity is associated with the solution of some 2D problems related to the calculation of the function $X_i(\mathbf{x})$ and a series of 1D problems for calculating the remaining functions involved in Eq 12. An alternate directions fixed point algorithm, with rank-one updates, that is, computing a term of the sum (Eq 12) at each iteration, is used to construct the temperature separated representation. Interested readers can refer to [30] and the references therein. The simulation configuration was the same as the one extensively considered in our former works [31].

3.2. *Model calibration*

According to [32], we first consider $L_x = 1$ m, $L_y = 6$ mm, the velocity of the laminate is $\mathbf{v} = 0.12$ m/s and the power source $P = 1000$ W. The point of contact between the roller and the mandrel is placed at $x_r = 0.8$ m (with $x = 1$ the incoming boundary). The conductivity along the fiber direction is set to $K_{xx} = 5$ W/mK and the ambient temperature is considered $T^{amb} = 22$ °C.

The composite heat capacity is calculated from the fiber volume fraction using the rule of mixtures as follows,

$$\rho C_p = w_f \rho_f C_{pf} + (1 - w_f)\rho_m C_{pm} \tag{13}$$

where w_f is the weight fraction of the fiber obtained from the image analysis. $C_{pf} = 1129$ J/kgK is the fiber specific heat capacity whereas $C_{pm} = 2200$ J/kgK is the specific heat capacity of the matrix. These values were collected from the suppliers specifications. On the other hand $\rho_m = 1300$ kg/m^3 is the matrix density, $\rho_f = 1790$ kg/m^3 and $\rho_f = 1700$ kg/m^3 are the fiber density for material A and material B, respectively.

Thus, a parametric solution is obtained with the material parameters (e, k_{yy}, k_{zz} and ρC_p) as extra-coordinates. Considering the mean values of the material parameters, the values of all transfers coefficients were fitted from the experimental measurements, i.e., for BT46, see Figure 7 [20]. This allowed to calibrate the model, in order to introduce the materials variability and study their influence on the thermal response as described in the next section.

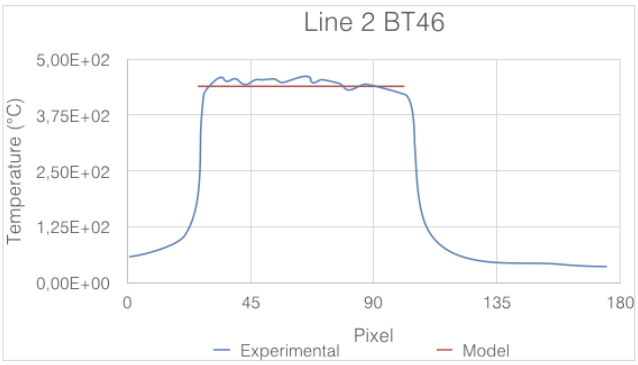

Figure 7. Comparison between the experiment thermal measurements (blue) and the numerical model (red) for sample BT46.

4. Stochastic framework

The aim of this section is to quantify the material uncertainty and its propogation. The stochastic simulation approach considered in this work is based in most standard formulation of the Monte Carlo (MC) method [33]. Monte Carlo simulation is a method for iteratively evaluating a deterministic model using sets of random numbers as inputs. Then the statistical characteristics of the model outputs are obtained, and their impact in the process is evaluated.

In each numerical experiment, the possible values of the input random variables $\mathbf{X}(X_1, X_2, ..., X_n)$ are generated according to their distributions shown in Section 2.

The Monte Carlo method presents a robust but usually computational expensive method as N simulations must be performed. However, in our case, the parametric solution already computed can be particularized for any choice of parameters without requiring further calculations, therefore Monte Carlo simulations become almost a real-time postprocessing.

Thus, $N = 10000$ realizations of the stochastic process were considered in the Monte Carlo analysis. The region of the parametric domain analyzed is considered as the surroundings the measurements taken in [20]. In the numerical simulation it corresponds to the volume $x \in [0.835, 0.855], y \in [0.0024, 0.0036]$ and $z = \frac{1}{4}e$. The temperature is averaged in that region and each value is plotted in Figure 8. The input random variables (k_{yy}, k_{zz}, e and ρC_p) are generated according to the distributions shown in Tables 1 and 2 for material A and material B, respectively.

Monte Carlo simulations are carried out for material A and material B. In Table 3, different statistical results are shown: sample mean, standard deviation, kurtosis and skewness. Figure 8 shows more dispersion in the temperature results for material B than for material A. Thus, for the same process conditions as material B reaches higher temperature values it could thermally degraded. This situation does not occur for material A, although the mean values for both materials are similar as shown in Table 3. The histogram, as shown in Figure 9, is a graphical representation of the distribution of numerical data and is an estimation of the probability distribution of a continuous variable (quantitative variable).

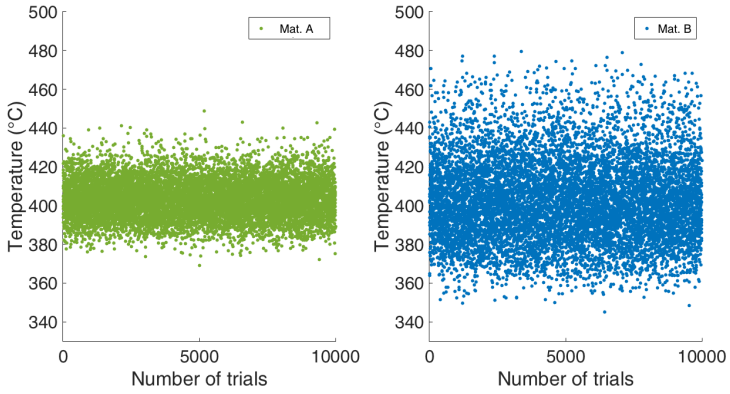

Figure 8. Monte Carlo thermal simulations (Averaged temperature in the zone of interest).

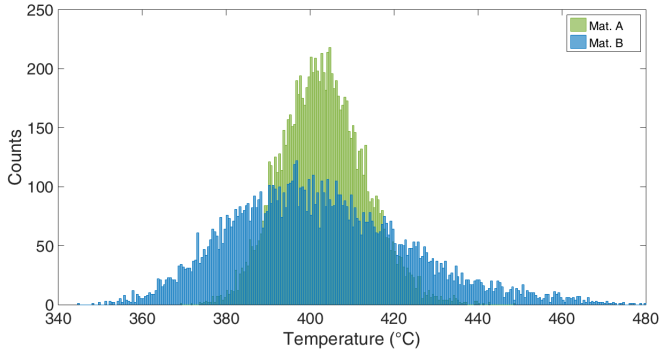

Figure 9. Histograms from simulations.

Table 3. Monte Carlo simulation results for ring setup.

Parameter	Temperature (°C) for material A	Temperature (°C) for material B
Mean, μ	403.19	402.43
Std dev, σ	9.98	21.15
Kurtosis	3.13	3.12
Skewness	0.25	0.48

Considering that, in the numerical simulation, $x = 0.8$ m is the contact point between the roller and the mandrel, the values from $x = 0.6$ to $x = 0.8$ m correspond to the consolidated tape and from $x = 0.8$ to 0.87 m the zone heated by the laser. Figures 10 and 11 show the temperature field from the MC simulation with respect to the tape placement direction, from $x = 0.6$ to $x = 0.87$ m for materials A and B respectively. The averaged temperature experienced by the material at the 1st interface is shown with a solid line, the maximum temperature with a dashed line and the minimum with a dash-dotted line.

Experiments were carried out for both materials A and B. The tapes of about 12 mm width were heated by using a laser of 200 W (wavelength 980 nm). The temperature on the incoming tape surface was measured by using a IR camera FLIR A655, 7–14 μm spectral range, 640 $\times$ 480 pixels resolution (1 pixel = 17 μm), 50Hz sampling frequency and 100–650 °C temperature range. Thus, the temperature along the incoming tape width at the hottest location was measured.

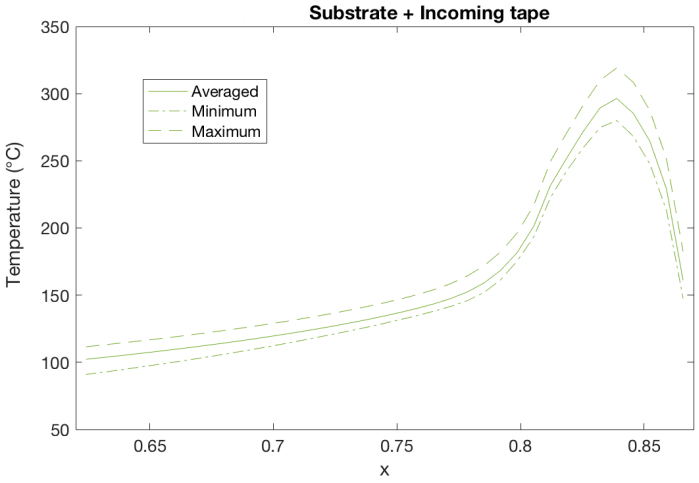

Figure 10. Averaged temperature along deposition direction (from right to left) of the incoming tape and the substrate for material A. We consider the frame attached to the laying head, and consequently the right boundary corresponds to the material inlet and the left one to the outlet.

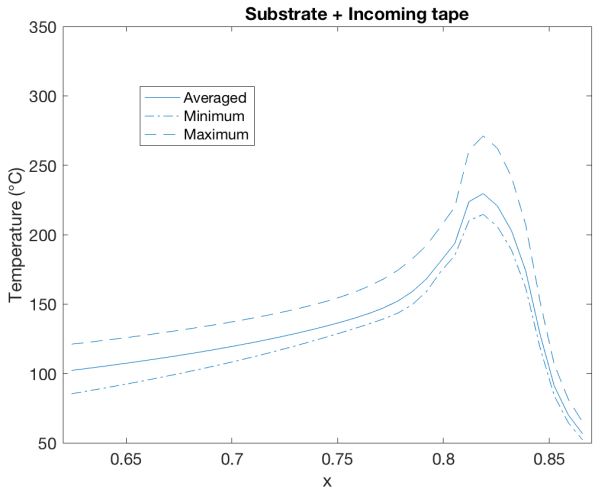

Figure 11. Averaged temperature along deposition direction (from right to left) of the incoming tape and the substrate for material B. We consider the frame attached to the laying head, and consequently the right boundary corresponds to the material inlet and the left one to the outlet.

Figure 12 depicts the incoming tape for both materials A and B, the heated region by the laser and the line along which temperatures were measured (Line 2). As it can be noticed in that figure, there is a certain temperature fluctuation across the tapes width, larger for material B. Such a fluctuation could evidence the intrinsic spatial variability of the parameters previously mentioned (thickness, thermal conductivity, local fiber concentration, etc ...), justifying that as discussed, material B having larger properties variability exhibits larger spatial fluctuations. The fluctuation interval for material B is of about 80 °C, i.e., $\Delta T_B^{Exp} \approx 80$ °C, being of about 50 °C the one related to material A, i.e., $\Delta T_A^{Exp} \approx 50$ °C.

Now, considering the numerical predictions for both materials referred to the incoming tape, Figure 13 depicts the temperature evolution along the tape length, being the hottest location the one associated with the coordinate $x = 0.85$ m, where the laser directly applies. At that location and due to the properties variability, temperature exhibits a variability in the intervals of length $\Delta T^{Fluct}_{A,x=0.85}$ for material A and $\Delta T^{Fluct}_{B,x=0.85}$ for material B, of magnitude 50 °C and 100 °C respectively (again the larger variability of material B properties justifies its larger interval of possible temperatures).

Experimental and numerical intervals of temperature fluctuation shown in Figures 12 and 13 respectively are in quite good agreement and could constitute a first qualitative proof of the modeling framework here proposed. As just indicated these results are very preliminary and consequently a deep experimental campaign is in progress to better quantify these tendencies.

In all the cases, if we compare material A with material B, there is more variability in the thermal response of material B, because of its heterogeneity. It would be interesting in further analyses to fix the desired temperature gap in a control zone ensuring an optimal deposition. This could allow us to give, for a fixed set of process parameters, a target variability for the different material parameters in order to ensure a right processability. Moreover, all the previous information doesn't allow to say which is the material parameter that has more influence on the temperature values. For addressing this question, a sensitivity analysis is carried out.

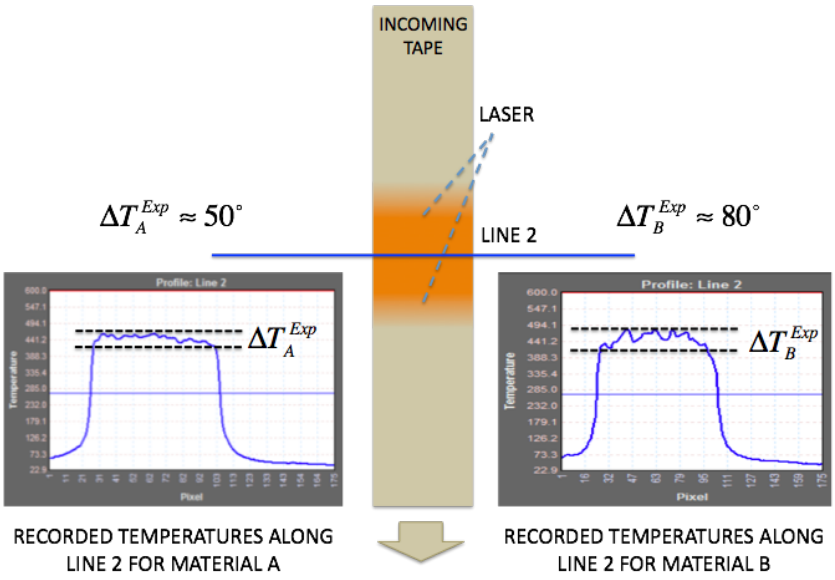

Figure 12. Temperature measurement along the tapes width for both materials at the hottest location (Line 2).

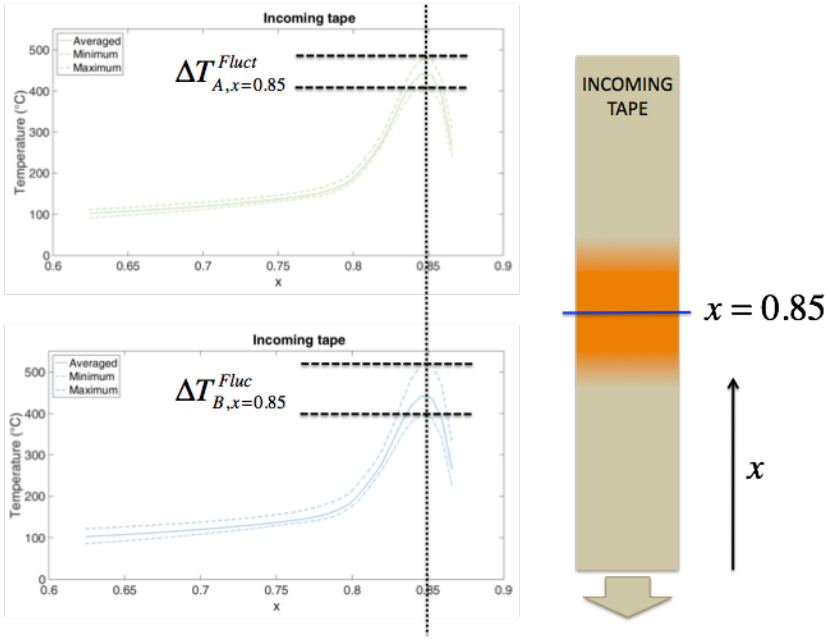

Figure 13. Temperature prediction along the tapes length and evaluation of the intervals of hottest temperatures at location $x = 0.85$ m.

However, addressing sensitivities experimentally is difficult because varying a given parameter without affecting all the other remains reasonably impossible. Numerical simulation offers such a possibility for performing sensitivity analyses, because modifying a parameter without modifying the others becomes strait-forward.

4.1. Sensitivity analysis

The sensitivity analysis performed in this section expresses how much would a parameter variation in the input of the model affects the thermal field output. This analysis identifies the most important parameters affecting the output. The sensitivity of the output, here the temperature T with respect to any of the input parameter, here the material parameters, is defined as the derivative of T with respect to the parameter. One may note that by using the PGD and thanks to the separated form of the temperature expressed by Eq 12, the sensibilities calculation becomes straightforward. For example, if one wishes taking the derivative of the temperature T with respect to the tape thickness e, it suffices to take the derivative of functions E_i with respect to e, i.e.:

$$\frac{\partial T}{\partial e} \approx \sum_{i=1}^{i=N} X_i(\mathbf{x}) \cdot Z_i(z) \cdot K_i^{yy}(k_{yy}) \cdot K_i^{zz}(k_{zz}) \cdot \frac{\partial E_i(e)}{\partial e} \cdot R_i(\rho C_p). \tag{14}$$

The temperature separated representation in Eq 14 involves few tens of modes and meshes are fine enough for ensuring the solution convergence.

Because the derivatives with respect to the different parameters involve different units, their comparison becomes delicate. For that reason the derivatives are normalized by giving the percentage on the temperature change with respect to a percentage of change of the involved parameters, allowing a proper comparison.

The sensibilities in this section are computed for $K_{yy} = 0.465\ W/mK$, $K_{zz} = 0.51\ W/mK$, $e_p = 0.1352\ mm$, and $\rho C_p = 2.56 \times 10^6\ J/m^3K$. The sensitivity with respect to the tape thickness is illustrated in Figure 14. In it, we can notice a negative sensitivity just above the heating zone, in the new added tape and below the heating region in the already consolidated layers. Therefore, at these locations and for those reference parameters values, increasing the tape thickness would decrease the temperature. Otherwise, the sensitivity is positive elsewhere in the part, and the effect is more pronounced on the steady state value of the temperature that corresponds to the left domain boundary. As discussed later, the tape thickness sensitivity is the highest with respect to all the sensibilities. Thus, 1% of change of it produced changes up to 1% in the temperature. Because the tape thickness can exhibit variations up to 20%, the variations in temperature will reach similar orders of magnitude.

The sensitivity to ρC_p is depicted in Figure 15. Tendencies are similar to the ones related to the tape thickness. However, the percentage of variation of the specific heat being much smaller than the one related to the thickness, its final effect will be less significant.

For the same parameters values, the sensitivity with respect to the in plane conductivity (in the direction orthogonal to the fibers) K_{yy} and the out-of-plane one K_{zz} are depicted in Figures 16 and 17 respectively. We can note that the K_{yy} variation has a negligible sensitivity in almost all the domain, as a 1% change in this parameter input only affects the temperature by 10^{-3}%. That result is not surprising as the process, due to the geometry of the prepreg tape (very thin layers compared to the in-plane dimensions) is mostly driven by out-of-plane thermal exchanges. The sensitivity to the

out-of-plane conductivity is as expected higher, as Figure 17 reveals. Thus, an increase of K_{zz} of 1% will induce a slight positive variation on the temperature (10^{-1}%) just above the heating zone in the new added tape and below the heating region in the already consolidated layers. However, in the already consolidated layers, increasing K_{zz} will slightly decrease the temperature in the rest of the domain. Because the noticed variability of the out-of-plane conductivity of about 10%, more significant variations are expected in the temperature.

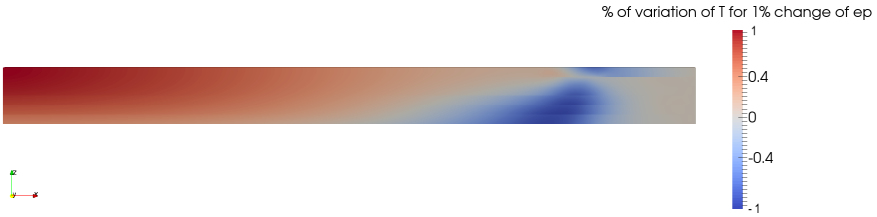

Figure 14. Temperature sensitivity with respect to the thickness of the tape. Variation of Temperature (in %) for a variation of 1% of the thickness value. We consider the frame attached to the laying head, and consequently the right boundary corresponds to the material inlet and the left one to the outlet.

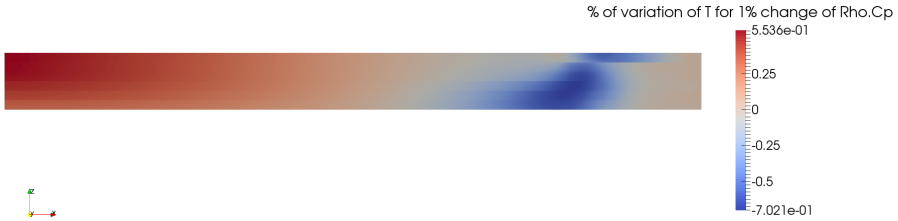

Figure 15. Temperature sensitivity with respect to ρC_p. Variation of Temperature (in %) for a variation of 1% of the ρC_p value. We consider the frame attached to the laying head, and consequently the right boundary corresponds to the material inlet and the left one to the outlet.

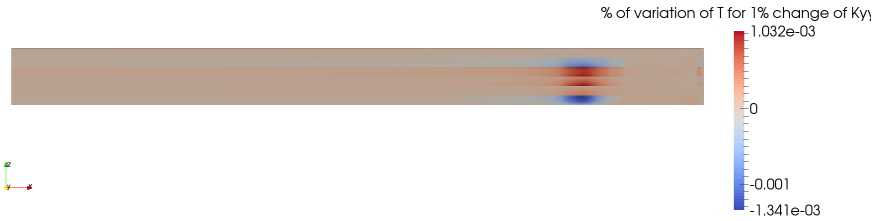

Figure 16. Temperature sensitivity with respect to K_{yy}. Variation of Temperature (in %) for a variation of 1% of the K_{yy} value. We consider the frame attached to the laying head, and consequently the right boundary corresponds to the material inlet and the left one to the outlet.

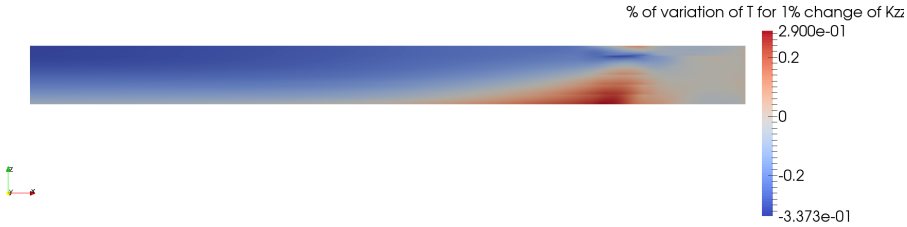

Figure 17. Temperature sensitivity with respect to K_{zz}. Variation of Temperature (in %) for a variation of 1% of the K_{zz} value. We consider the frame attached to the laying head, and consequently the right boundary corresponds to the material inlet and the left one to the outlet.

In summary, the parameter having the highest impact on the temperature field are the thickness and ρC_p parameters, with the thickness having a much more pronounced effect as this parameter presents a high variability. Then the through-the-thickness thermal conductivity parameter comes in second order, as either its variation and also its impact are lower, and finally the in-plane thermal conductivity (in the direction orthogonal to the fibers) is totally negligible.

5. Concluding remarks

The main aim of this work was to study the influence of material parameters variability in the thermal behaviour during the LATP process. The material parameters analyzed were the thickness, the fiber volume fraction (directly related to the parameter ρC_p in the numerical model) and the homogenized conductivity tensor in the cross-section of the tape (k_{yy} and k_{zz}). Microscopic cross-sections were analyzed, allowing to characterize the material variability from two different suppliers. This characterization showed a higher variability for the material B supplier than for the material A, which might have an influence on the thermal response.

On the other hand, temperature measurements were carried out with a thermal camera during deposition, allowing to extract different informations (either by inverse analyses, the values of the thermal exchanges parameters, and also to identify the thermal variation of the temperature during the deposition on the tape). For that purpose most of experimental measurements were performed along the width of the tape in the hottest zone. It might be interesting to extend this measurements at different locations of the process, e.g., near the contact between roller and mandrel, in order to improve the confidence in the proposed simulation tool.

Moreover, the simulation tool allowed to conduct very efficiently a stochastic analysis based on the Monte Carlo method (only by post-treatment of the data with a PGD-based parametric solution) in order to quantify the material variability impact on the thermal response. By comparing the two materials, we concluded that the higher dispersion in the material and process parameters, the more dispersion in the temperature values experienced by the material during its forming stage. Finally, a sensitivity analysis was carried out in order to identify the most critical parameters on the thermal response. As expected the material thickness appears as very significant, as well as the through-the-thickness thermal conductivity k_{zz}, and the ρC_p parameter. The last one having an impact localizing in the cooling domain, whereas k_{zz} present a more local impact under the heating zone, whereas the material thickness impact appears either in the heating zone and the cooling regions. Moreover, it

can reasonably stressed that the in-plane thermal conductivity k_{yy} has no significant impact on the temperature field.

In summary, the results presented here show that material uncertainty can introduce significant variability in the thermal response with considerable impact in industrial practice. Consequently, variability effects should be incorporated in process design/optimization to ensure robustness.

A deeper sensitivity analysis coupled with temperature range recommandation in order to ensure a good deposition quality could provide precious indications for material parameters specifications and constitutes a work in progress.

Conflict of interest

The authors declare that they have no conflict of interest.

References

1. Kollmannsberger A, Lichtinger R, Hohenester F, et al. (2017) Numerical analysis of the temperature profile during the laser-assisted automated fiber placement of CFRP tapes with thermoplastic matrix. *J Thermoplast Compos*.
2. Schaefer P, Gierszewski D, Kollmannsberger A, et al. (2017) Analysis and improved process response prediction of laser-assisted automated tape placement with PA-6/carbon tapes using design of experiments and numerical simulations. *Compos Part A-Appl S* 96: 137–146.
3. Yassin K, Hojjati M (2017) Processing of thermoplastic matrix composites through automated fiber placement and tape laying methods: A review. *J Thermoplast Compos*.
4. Schledjewski R, Latrille M (2003) Processing of unidirectional fiber reinforced tapes—fundamentals on the way to a process simulation tool (ProSimFRT). *Compos Sci Technol* 63: 2111–2118.
5. Grouve W (2012) Weld strengh of laser-assisted tape-placed thermoplastic composites [PhD thesis]. University of Twente.
6. Stokes-Griffin C, Compston P, Matuszyk T, et al. (2015) Thermal modelling of the laser-assisted thermoplastic tape placement process. *J Thermoplast Compos* 28: 1445–1462.
7. Reichardt J, Baran I, Akkerman R (2018) New analytical and numerical optical model for the laser assisted tape winding process. *Compos Part A-Appl S* 107: 647–656.
8. Stokes-Griffin C, Ehard S, Kollmannsberger A, et al. (2017) A laser tape placement process for selective reinforcement of steel with CF/PA6 composites: Effects of surface preparation and laser angle. *Mater Design* 116: 545–553.
9. Dedieu C (2017) Towards mastering the filament winding process with in situ consolidation for launcher application [PhD thesis]. Ecole Centrale de Nantes.
10. Dedieu C, Chinesta F, Barasinski A, et al. (2016) Model of laser/composite interaction based on scattering by multiple cylinders. *AIP Conf Proc* 1769: 170021.
11. Dedieu C, Barasinski A, Chinesta F, et al. (2017) On the prediction of residual stresses in automated tape placement. *Int J Mater Form* 10: 633–640.

12. Dedieu C, Barasinski A, Chinesta F, et al. (2017) About the origins of residual stresses in in situ consolidated thermoplastic composite rings. *Int J Mater Form* 10: 779–792.
13. Saoudi A, Leon A, Gregoire G, et al. (2017) On the interfacial thermal properties of two rough surfaces in contact in preimpregnated composites consolidation. *Surf Topogr-Metrol* 5: 045010.
14. Leon A, Barasinski A, Abisset-Chavanne E, et al. (2018) Wavelet-based multiscale proper generalized decomposition. *CR Mécanique* 34: 485–500.
15. Leon A, Barasinski A, Nadal E, et al. (2015) High-resolution thermal analysis at thermoplastic pre-impregnated composite interfaces. *Compos Interface* 22: 767–777.
16. Deignan A, Figiel L, McCarthy M (2018) Insights into complex rheological behaviour of carbon fibre/PEEK from a novel numerical methodology incorporating fibre friction and melt viscosity. *Compos Struct* 189: 614–626.
17. Algerich C, Leon A, Ibanez R, et al. (2018). Prediction of composites behavior undergoing an ATP process through data-mining. *AIP Conf Proc* 1960: 020016.
18. Leon A, Argerich C, Barasinski A, et al. (2018) Effects of material and process parameters on in-situ consolidation. *Int J Mater Form* [in press].
19. Van Hoa S, Duc Hoang M, Simpson J (2017) Manufacturing procedure to make flat thermoplastic composite laminates by automated fibre placement and their mechanical properties. *J Thermoplast Compos* 30: 1693–1712.
20. Fouyer K (2016) Etude de la variabilité des caractéristiques thermiques des tapes de pré-imprégnés dans le cadre de l'enroulement filamentaire thermoplastique [Master dissertation]. Ecole Centrale de Nantes.
21. Trias D, Costa J, Turon A, et al. (2006) Determination of the critical size of a statistical representative volume element (SRVE) for carbon reinforced polymers. *Acta Mater* 54: 3471–3484.
22. Lopez E, Abisset-Chavanne E, Lebel F, et al. (2016) Advanced thermal simulation of processes involving materials exhibiting fina-scale microstructures. *Int J Mater Form* 9: 179–202.
23. Hatta I, Yamane T, Katayama S, et al. (2000) The measurements of thermal conductivity of carbon fibers. *J Wide Bandgap Mater* 7: 294–305.
24. Tian T (2011) Anisotropic thermal property measurements of carbon-fiber/epoxy composite materials [PhD thesis].
25. Zhang X, Fujiwara S, Fujii M (2000) Measurements of thermal conductivity and electrical conductivity of a single carbon fiber. *Int J Thermophys* 21: 965–980.
26. Grujicic M, Zhao C, Dusel E, et al. (2006) Computational analysis of the thermal conductivity of the carbon–carbon composite materials. *J Mater Sci* 41: 8244–8256.
27. Ghnatios C, Mathis C, Simic R, et al. (2017) Modeling soft, permeable matter with the Proper Generalized Decomposition (PGD) approach, and verification by means of nanoindentation. *Soft Matter* 13: 4482–4493.
28. Ghnatios C, Xu G, Leygue A, et al. (2016) On the space separated representation when addressing the solution of PDE in complex domains. *Discrete Cont Dyn-S* 9: 475–500.

29. Chinesta F, Ammar A, Cueto E (2010) Recent advances and new challenges in the use of the Proper Generalized Decomposition for solving multidimensional models. *Arch Comput Method E* 17: 327–350.
30. Chinesta F, Keunings R, Leygue A (2014) *The Proper Generalized Decomposition for advanced numerical simulations: A primer*, Springer International Publishing.
31. Chinesta F, Leygue A, Bognet B, et al. (2014) First steps towards an advanced simulation of composites manufacturing by automated tape placement. *Int J Mater Form* 7: 81–92.
32. Courtemanche B, Fouyer K, Barasinski A (2018) Influence des propriétés thermiques des pré-impregnés composites thermoplastiques pour l'enroulement filamentaire laser. *Revue des Composites et des Matériaux Avancés* 28: 69–88.
33. O'Hagan A (2013) Polynomial Chaos: A Tutorial and Critique from a Statistician's Perspective. Available from: http://www.tonyohagan.co.uk/academic/pdf/Polynomial-chaos.pdf.